Advanced Steel Construction – Vol. 18 No. 1 (2022) 436–445
DOI:10.18057/IJASC.2022.18.1.2

THE SEISMIC PERFORMANCE OF DOUBLE TUBE BUCKLING RESTRAINED BRACE WITH CAST STEEL CONNECTORS

Zhan-Zhong Yin [1, 2, *], Da-Zhe Feng [1], Bo Yang [1] and Chao-Chao Pan [1]

[1] *School of Civil Engineering, Lanzhou University of Technology, Lanzhou 730050, China*
[2] *Western Engineering Research Center of Disaster Mitigation in Civil Engineering of Ministry of Education, Lanzhou University of Technology, Lanzhou 730050, China*
[*] *(Corresponding author: E-mail: yinzhanzhong@lut.edu.cn)*

ABSTRACT

The special concentrically braced frame (SCBF) is an aseismic structure, but its bracing system exhibits brittle failure and premature buckling connected with the weld fracture of the gusset plate and the post-buckling of the braces; thus, maximizing the role of energy dissipation is difficult. Here, this paper proposes a system of double-tube buckling-restrained brace with cast steel connectors for steel SCBFs. The large inelastic deformation of the bracing system is mainly concentrated in the ductile cast connectors under the earthquake, and the degree of buckling and post-buckling of braces can be reduced. Cyclic loading tests were conducted on two groups of specimens with different parameters, then the deformation trend, stress distribution, energy dissipation capacity, and stiffness degradation of the specimens were analyzed. The improved measures of increasing the width–thickness ratio of the energy dissipation plate and stiffener and casting the end right-angle tip tightly for a certain length of cast connector in Group 2 specimens, which overcomes the brittle fracture caused by the crack of the connection segment due to flexural buckling in Group 1 specimen tests, was evaluated. The cast steel connector conducts the main energy dissipation member that exhibits good ductile and energy absorption performance, and the advantages of using improved ductile cast steel connectors to obtain the energy dissipation of BRBs are illustrated. The test results provided direct evidence that the seismic performance of specimens is closely associated with the length of the energy dissipation segment of the cast connector and the overstrength factor of axial force. Also, the strength, rigidity, deformation, and energy dissipation performance of the members can be independently controlled by reasonably designing the cast connector. Our results provide the underlying insights needed to guide the design of the bracing connector.

ARTICLE HISTORY

Received: 17 April 2021
Revised: 24 May 2021
Accepted: 24 May 2021

KEYWORDS

Buckling restrained brace;
Cast steel connector;
Cyclic loading test;
Seismic performance;
Special concentrically braced frame

1. Introduction

A special concentrically braced frame (SCBF) [1] is a steel structural system with a high bearing capacity and a large lateral stiffness. However, the Kobe earthquake in 1995 [2] exposes the problem of SCBF structures inevitably suffering from buckling and fracture of the bracing system. Notably, an intensive review found that the fracture failure of bracing mainly occurs at the end connection. Before that, Goel et al. studied the concentrically braced frame system with various types of supports connected by gusset plates and found that gusset plates are prone to brittle failure [3,4]. Subsequently, several studies and reviews focused only on the mechanical behavior of gusset plate connectors [5-9], whereas the effects of support on the gusset plate have not been considered for many years. These trends led to a proliferation of studies on the yield mechanism, inelastic deformation capacity, and ultimate failure mode of bracing members with end connectors over the past two decades. Tremblay et al. conducted extensive research on the mechanical properties of steel bracing under cyclic loading [10] and found that the aspect ratio and slenderness ratio are the most important parameters that affect the life of the support. Similar work was conducted by Shaback and Brown [11], who proposed the calculation formula of the life of hollow structural steel section (HSS) support. Tests were conducted on a two-layer frame with an HSS cross-section brace by Uriz et al. [12], who found that this brace would lead to fracture at the beam-column joints. Moreover, Roeder et al. [13,14] studied the seismic design of frame support structures and found that the lateral displacement capability and the ductility of the structure can be greatly improved by controlling the yielding of braces and connectors. Although the frame structure has certain ductility, the deformation capacity of the brace is often limited due to premature yielding [15].

The problem of insufficient energy dissipation of bracing system has attracted considerable attention to the performance of support, which is another key factor that affects the seismic performance of the SCBF structural system. Compared with traditional braces, buckling-restrained braces (BRB) are a kind of brace that relies on its core component that could be confined with a peripheral component from buckling to achieve full-section yield [16-18]. To release expansion and contraction of the core component in the vertical and horizontal directions, the core component and the peripheral component are required to retain a certain gap [19]. The gap is generally filled with filler materials to provide better-confined action [20-21]. As a part of their study, Sridhara et al. [22] proposed a brace with a casing pipe that confined the bending of the core member, thereby squeezing the peripheral pipe to generate flexural stress. The yield strength of the sleeve is greater than the flexural stress, thus improving the compressive bearing capacity of the core member. A comparison of different types of BRBs is given in [23], where the author claimed that the lack of adhesive materials such as mortar and concrete will lead to premature local buckling of the core component. This issue has been considered by recent work [24], in which the frictional force in the contact area of the core component increased and the strain distribution along the core member was not uniform, which were closely associated with increased clearance between the core component and the limiter under compressive load. This finding established that the clearance between the core component and the limiter plays an important role for evaluating the seismic performance of BRB. A proposed double steel tube buckling-restrained brace simplified the structure of the brace and made field installation more convenient [25,26]. Since then, Yin et al. [27] added a contact ring between the inner and outer components to improve the double-tube BRB. Finite component analysis and tests showed that this support has good energy dissipation performance, and the lateral stiffness of the inner tube confined with the contact rings is significantly improved [28,29]. Hence, this BRB could be introduced to SCBF systems to replace the traditional support to address the limitation of premature buckling.

Nonetheless, the energy dissipation performance of BRB has not yet been fully utilized due to the brittle failure of the gusset plate. A ductile connector is urgently needed instead of the gusset plate to avoid brittle failure of structural joints. Fleischman et al. [30] proposed a modular cast steel connector for steel moment frames, and the later work of [31] extended the ductility of the connector by geometrically based techniques. A conceptually similar study was conducted by [32], in which the cast connector was used as the end connector for HSS braces to avoid brittle failure. Gray et al. [33] offered a yielding brace system that dissipates seismic energy by flexural yielding of special cast connectors. The advantages of prefabricated modular steel construction in industrial technique enhanced productivity, site safety, and construction quality is evident. More recent work in this area [34] extends the methods by using a new type of bolted joint for modular steel building, which indicated that the joints have stable bearing capacity with adequate ductility and seismic performance. A similar connecting method was proposed in tests by [35], which considered that a connection with slot bolt holes revealed the potential application of these connections for a dual-function component in a structure to simultaneously provide stiffness and energy dissipation capacity.

Current research on modular ductile connectors tends to focus on beam-column joints or traditional braces rather than BRBs. However, it has not explicitly addressed the issue of premature buckling and low dissipation of the brace. A systematic understanding of how ductile cast connector contributes to the BRB is still lacking. Considering the assembling of prefabricated buildings need for a precise connecting system to ensure structural integrity and effective

transfer of loads and moments, an assembling modular connector for BRBs needs to be developed. This paper presents a bracing system of buckling-restrained brace with cast connectors (CBRB), where ductile cast steel connectors are used for double-tube BRB with contact rings instead of the gusset plate to alleviate the stress concentration of the joint. Low cycle loading tests were performed on the members, and the impact of different parameters of cast connectors on the mechanical properties and energy-dissipating performance for specimens were analyzed. Using the excellent ductility of cast connectors to avoid brittle failure of connector for the brace enabled the BRB to fully exert energy dissipation. An equally important detail is that the cast connector can act as the main energy dissipation component to concentrate most of the inelastic deformation of members, which enables the structure to dissipate energy in stages and prolongs the time course of energy dissipation. In addition, the cast connector can be a "fuse" for easy replacement to reduce the inspection time and repair cost of structures after an earthquake. This work provides a new idea for the application of assembled connectors, which has important theoretical significance and broad engineering application prospects.

2. Theoretical analysis for design of cast connector

The energy-dissipating brace is an axially deformable member that provides lateral stiffness for SCBFs. Therefore the design method based on the lateral stiffness ratio could be applied for the steel frame system with BRB. As shown in Fig. 1, the configuration after deformation is identical to the initial configuration of the frame on the basis of an assumption concerning the small deformation in the theory of elastoplasticity. Therefore, the angle between the support and the horizontal direction, θ, in the structure can be assumed to be the same before and after deformation. Theoretically, the axial displacement of support ΔL can be calculated according to Equation (1)

$$\Delta L = \cos\theta = \frac{FL}{EA} \tag{1}$$

In Equation (1), F is the axial force in the support, A is the cross-sectional area of the support, and E is the Young's modulus. Thus, the horizontal component for the axial force of brace is

$$F_n = F\cos\theta = \frac{EA\cos^2\theta}{L} \tag{2}$$

The lateral stiffness of BRB is

$$K_D = F_n/1 = EA\sin\theta\cos^2\theta/h \tag{3}$$

The nominal rigidity ratio is defined as $k = K_D/K_f$. K_f is the lateral stiffness of steel frame obtained by the D-value method with $K_f = 12\gamma E_c I_c/h^3$, γ is the correction coefficient, E_c is the Young's modulus of the column, I_c is the moment of inertia of the column, and h is the height of the column. The effect of reasonable lateral stiffness ratio on the seismic behavior of steel frame structures with braces is self-evident. According to the finite component analysis of the influence of the lateral stiffness ratio on the whole steel frame structure was completed by Liu [36], support does not affect the whole frame, as the lateral stiffness ratio exceeds 2.5. According to the above statement, the sectional area of the inner tube of BRB can be obtained, that is,

$$A = k\cdot K_f\cdot h/E\sin\theta\cos^2\theta \tag{4}$$

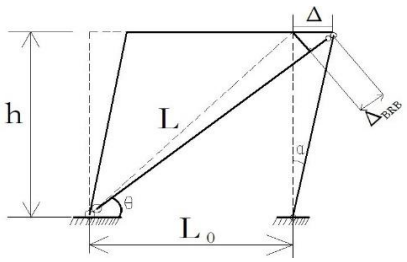

Fig. 1 Schematic of BRB deformation

As minor deformation occurs, Fig. 1 shows that $\Delta = h\tan\alpha$, $\cos\theta = L_0/L$ and $L = \sqrt{L_0^2 + h^2}$. Thus, the total deformation of a single diagonal BRB can be expressed as

$$\Delta_{BRB} = \Delta\cos\theta = h\tan\alpha\cos\theta = \tan\alpha L_0 h/L \tag{5}$$

According to Equation 5, the story drift, α, can be used to calculate the deformation of the bracing member. It is important to highlight that the elastic–plastic story drift of 1/50 specified in the Chinese code [37] should be adopted to design deformable components, while the elastic story drift under the frequent earthquakes does not ensure that all energy-dissipating members yielded. Thus, as the axial displacement of the support, $\Delta_{plastic}$, is

As shown in Fig. 2, both ends of BRB are connected with the frame through ductile cast connectors arranged at the connection zone to form an SCBF system. Using the ductile cast connector instead of the gusset plate is advantageous for energy dissipation. Therefore, the plastic deformation of the system could be concentrated on the ductile cast connector as much as possible through a reasonable detailed design of the energy dissipation member. Fig. 3 presents a schematic of the structure of ductile cast connector and cross-sectional shape of energy dissipation segment. The ductile cast connectors can be designed into a cross-section with three parts: L1 is the connection segment, which was designed as a right-angle tip for easy frame connection; L2 is the actual energy dissipation segment that drawing on the "dog bone" idea of the weakened segment; and L3 is the transition segment connecting with the brace. The energy dissipation segment enhances the strength of the connection and transition segments to a certain extent. Therefore, the stress distribution of the beam-column joint will not change due to the large stiffness of the connection segment as the brace is damaged.

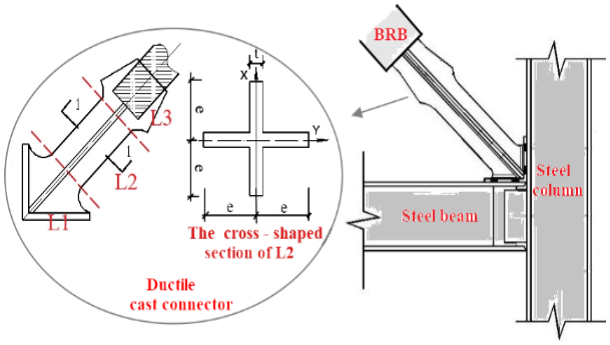

Fig. 2 Schematic of ductile cast connector

The deformation of the cast connector is mainly concentrated on the energy dissipation segment, of which the section is cross-shaped and prone to torsional buckling. For cross-section, its torsional buckling load P_{cr} is as follows:

$$P_{cr} = \frac{GI_t}{i^2}\left(1 + \frac{\pi EI_w}{GI_t l^2}\right) \approx \frac{GI_t}{i^2} \tag{6}$$

In Equation (6), i is the radius of polar rotation of the star section with respect to the shear center; I_t is the torsional moment of inertia of the section; I_w is the warping moment of inertia of the cross-section; and G is the shear modulus. As a result of the pimping moment of warping inertia of the section is small, it can be ignored. Therefore, the ultimate load of torsional instability of the section can be approximately expressed as GI_t/i^2. where $G = E/2(1+\nu)$; $i^2 = \left(I_x + I_y\right)/A$. The torsional buckling stress of cast connector can be expressed as

$$\sigma_{cr} = \frac{P_{cr}}{A} = \frac{GI_t}{Ai^2} = \frac{E\cdot\frac{4}{3}et^3}{2(1+\nu)\cdot\frac{4}{3}e^3 t} = \frac{E}{2.6}\left(\frac{t}{e}\right)^2 \tag{7}$$

where e is the extended length of the cross-section, and t is the width of the plate for the cross-section. To avoid torsional buckling of ductile cast connectors, a necessary step is to ensure that $\sigma_{cr} \geq f_y$, in which f_y is the yield strength of cast connectors. Thus, $e/t \leq \sqrt{E/2.6 f_y}$ can be obtained. Assuming that all plastic deformation is concentrated on the weakened energy dissipation segment of the cast connector at both ends of the support, the minimum length of the energy dissipation segment of the cast connectors can be ascertained as

$$L_{2,\min} = \Delta_{plastic} / \delta \tag{8}$$

In Equation (8), δ is the elongation of the steel. The energy dissipation segment is the main axially compressed member, and the slenderness ratio λ_{L2} can be calculated as

$$\lambda_{L2} = \mu L_2 / i \tag{9}$$

where μ is the effective length factor. In this paper, μ=2 .

3. Experimental program

3.1. Test specimens

The specimen is based on a single-layer special concentrically braced frame with a span of 6 m and a height of 4. 5 m, in which the beams and columns are both H-section and rigidly connected, and both ends of the brace are hinged with beam-column joints. The beam and column dimensions are H400×300×10×16 and H400×400×12×20, respectively, and the lateral stiffness ratio K = 2. 8 of the frame was selected for brace validity. To further study the energy dissipation performance of cast connectors, the inner tube sections of BRBs for all specimens were designed to the same specification. The cross-sectional area of the inner tube was calculated as 2541 mm^2 by Equation (4) to this end. Fig. 3 provides an overview of double steel tube BRBs. The seamless steel tubes are used for all parts, and then both ends of BRB are provided with end plates to facilitate connection with cast connectors by high-strength bolts. The tests were performed with half of the whole member based on the symmetry of the system to help fix the specimen on the loading frame. The specific parameters are obtained from the geometric dimensions of BRBs in Table 1.

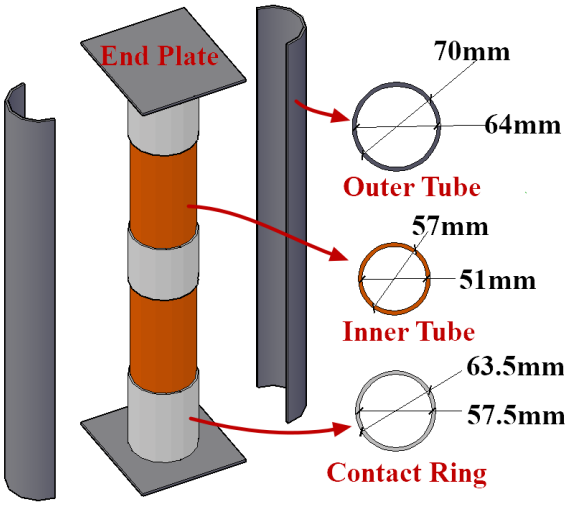

(a) Section design

(b) Member

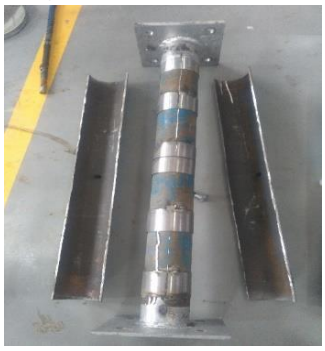

(c) Inner tube with contact rings

Fig. 3 Photo of BRB component

Table 1
Parameter table of BRBs

Inner tube section	Inner tube length/mm	Outer tube section	Outer tube length/mm	Contact ring section	Number of contact rings
Φ121×5.5	1300	Φ140×6.5	1180	Φ127×3	5

For the same reason, the end part of the transition section is provided with a connecting end plate where the cast connector is connected with BRB by a high-strength bolt to facilitate the replacement and repair of the cast connector. As shown in Table 2 and Fig. 4, eight cast connectors were made based on dimensions and length of the cross-shaped section, of which the wedge plate inscribed with the two legs of the right-angle steel is the main deformable component to dissipate energy, and the plate in the other direction could act as a stiffener. The direction along the energy dissipation plate is defined as x-axis corresponding to the direction along the stiffener as y-axis in the cross-section. The width–thickness ratios of stiffeners and energy dissipation plates can be used as a section parameter for easy analysis. The specific focus in Fig. 4a is the right-angle tip of the cast connector for some of the specimens. This right-angle tip was cast tightly below a certain height of L1 for end reinforcement, and the width–thickness ratios of the stiffeners and energy dissipation plates improved. This result occurred because the cast connectors in the Group 1 specimens exhibited untimely fracture during the loading process due to the flexural buckling of the connection segment. We expect our proposed solution will help address this issue. For this reason, only two specimens in Group 1 were taken for analysis, and the remaining improved six specimens were labeled as Group 2 for later tests. The corresponding yield load of each energy-dissipating component for designed specimens was obtained by performing finite component numerical simulation. The axial force overstrength coefficient of specimens, n , is defined as follows:

$$n = P_{y,c} / P_{y,b} \tag{10}$$

In Equation (10), $P_{y,b}$ is the axial yield load of the BRB, and $P_{y,c}$ is the axial yield load of the cast connector.

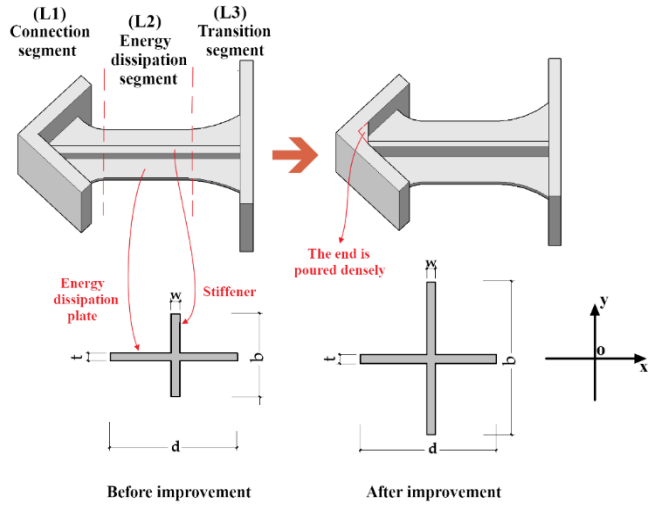

(a) Section design and improvement

(b) Specimens before improvement

(c) Specimens after improvement

Fig. 4 Cast steel connectors

Table 3 provides the material properties for the steel samples measured by the tensile coupon test. The test was conducted according to the Chinese “Metallic materials—Tensile testing at ambient temperature” (GB/T 228–2002) [38]. Fig 5 presents an overview of steel samples for components, and the representative value of each material property index was taken as the average value of the test results of each test sample. The samples for cast connectors are made of low-yield-point steel, whose strength is lower than that of BRB.

Table 1
Parameter table of specimens

Specimen grouping	Specimen Number	Specification of Cast connectors /mm							Total Length (mm)	Slenderness ratio of L2 λ_{L2}	Overstrength Coefficient n	Area ratio	End Reinforcement
		L1	L2	L3	t	w	b	d					
Group 1	CBRB-1	150	150	90	18	18	36	66	390	36.51	0.786	0.595	×
	CBRB-2	150	150	90	18	18	46	66	390	29.24	0.797	0.666	×
Group 2	CBRB-3	150	100	140	20	14	82	74	390	11.64	0.817	0.924	√
	CBRB-4	150	150	90	20	14	82	74	390	17.47	0.817	0.924	√
	CBRB-5	110	200	80	20	14	82	74	390	23.29	0.817	0.924	√
	CBRB-6	150	150	90	20	12	80	80	390	19.22	0.805	0.913	√
	CBRB-7	150	150	90	22	16	80	68	390	17.14	0.841	0.954	√
	CBRB-8	150	150	90	20	16	82	72	390	16.72	0.845	0.957	√

Note: "Area ratio" denotes "the ratio of the cross-sectional area of the energy dissipation segment to the inner tube of the BRB"

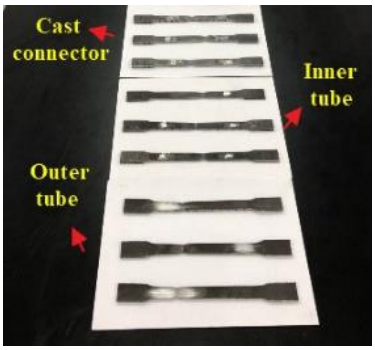

Fig. 5 Photo of steel samples

Table 3
Material parameters

Sample category	Steel grade	Yield strength (MPa)	Ultimate strength (MPa)	E_s (GPa)	Elongation (%)
Cast connectors	Q235	264	500	206	20
Inner tube	Q345	350	510	206	25
Outer tube	Q345	340	500	206	26

3.2. Instrumentation, test device, and loading protocol

Fig. 6 shows the loading device, which consists of a vertical portal loading frame, a hydraulic jack, a right-angle support, and a rigid base, where the right-angle support is a right-angle surface that simulates the beam-column joint. The two ends of the rigid base are fixed on the ground through pressure beams to prevent out-of-plane displacement of the member. The right-angle support and rigid base are connected by 10.9-grade high-strength bolts to fix the lower end of the specimens to ensure vertical loading. A heavy hammer line was hung in the vertical direction to observe the degree of inclination of the specimen during the loading process. To observe the deformation of the specimens in the vertical direction and the horizontal direction during the test more intuitively, horizontal and vertical guiding rulers are respectively arranged at the matching position of the cast connector and the lower end of the BRB.

Fig. 6a shows that 10 displacement meters are erected around the cast connector and BRB, and the deformation of the global specimen could be known by the displacement meter readings. To determine the stress distribution of the specimen during the test, resistance strain gauges are arranged on the cast steel connectors and BRBs. As shown in Fig. 7, strain gauges are arranged on both sides of the energy dissipation plate and stiffener of the ductile cast connector, which is mainly used for detecting various stress changes of the energy dissipation segment during the test. Also, strain rosettes are arranged on the connection segment and the transition segment to detect the stress at the portion where the sectional shape is changed. Given that the inner tube of BRB is the main energy-dissipating component, strain gauges are arranged along the length direction of the extended parts of the inner tube at both ends of the BRB.

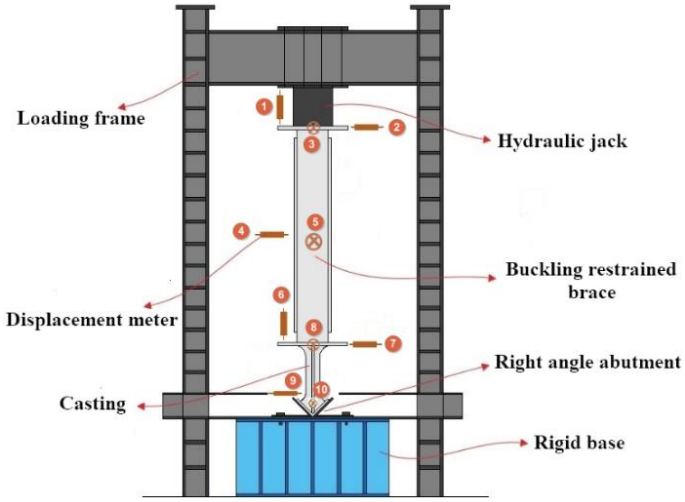

(a) Vertical portal loading frame and displacement meter arrangement

(b) Photo of the vertical portal loading frame

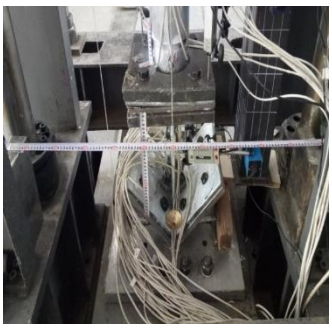

(c) Heavy hammer line and guiding rulers

Fig. 6 Loading device

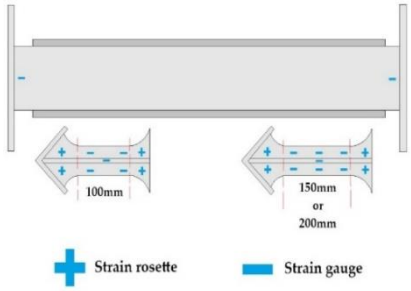

Fig. 7 Measuring arrangement of strain gauge and strain rosette

In the test, a 1000 kN electro-hydraulic servo system was used for axial cyclic loading to examine the hysteretic performance of cast connectors. The loading pattern in Fig. 8 shows the loading method of displacement control with

amplitudes of 2 mm, 4 mm, 6 mm, 8 mm ..., and each amplitude is loaded for three cycles at a time until the specimen is damaged. The axial compression and elongation rate of the total specimen, $\delta^{\pm}$, are defined as the ratio of the displacement exerted by the actuator to the total length of the specimen.

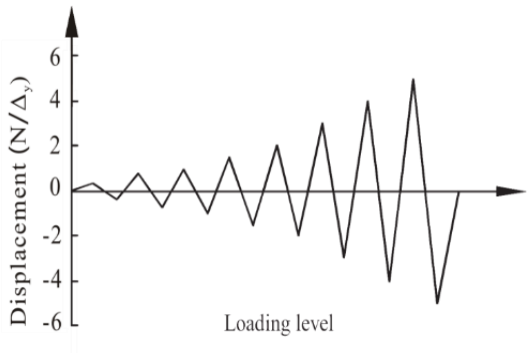

Fig. 8 Loading pattern

4. Experimental results and discussion

4.1. Damage processes and failure mode

All the specimens were in the elastic stage during the first two cycles of 2 mm loading displacement ($\delta^{\pm}=1/880$), and no obvious test phenomenon was observed. Starting from the third cycle, closer inspection of readings of both Nos. 9 and 10 displacement meters showed that the connection segment of CBRB-1 shifted for an approximately 2 mm out-of-plane displacement in the X and Y direction. Accordingly, the observed parallel results were that nearly 5 mm out-of-plane displacement of the upper end of BRB was measured by the No. 3 displacement meter. Similarly, these findings were observed in the testing of CBRB-2, and the out-of-plane displacement increases with the test process. This finding, while preliminary, suggests that flexural buckling occurred, which skewed the specimen toward the out-of-plane. From the data in vertical displacement meters, it is apparent that each component of the specimen begins to undergo axial tension and compression deformation. A review of the readings showed that the deformation increases with the raising of the test load. As the loading displacement approached 6 mm ($\delta^{\pm}=1/293$), the transverse cracks appeared at the coating of the connection segment of cast connectors of the specimen CBRB-2 and CBRB-1 successively. The cracks continued to develop and increase, and a slight coating warping was found around the cracks as the test progressed. Further comparison of displacement meter readings revealed that the compression and elongation of BRBs are less than those of ductile cast connectors. When the loading displacement reached 6.6 mm ($\delta^{-}=1/267$), a crack was found at one side of the energy dissipation plate axis of connection between the connection segment and the right-angle steel of CBRB-2. This result could be attributed to the inclination of the cast connector mainly on one side of the Y direction. After a short time, the coating bulged in the energy dissipation segment and cracks appeared gradually, and numerous cracks were significant at $\delta^{\pm}=1/196$. The endplate between the BRB and the cast connector of CBRB-1 skewed 4 mm toward the out-of-plane in the direction of the x-axis at the moment. As the loading displacement further increased, the cast connector of CBRB-2 was excessively stretched vertically. When the displacement finally reached −10 mm ($\delta^{-}=1/176$), the cracks at the paint coating of the energy dissipation plate widened, and the paint skin began to fall off in a large area. Subsequently, the crack on one side of the end of the connection segment of the cast connector ran through, and then the crack developed in the other side afterward. When the hydraulic jack finally returned to the equilibrium position, one side of the end of the CBRB-2 connection segment fractured (Fig. 9c). Meanwhile, the specimen CBRB-1 was severely inclined (Fig. 9a). As shown in Fig. 9b, cracks appeared at both sides of the energy dissipation plate axis of connection between the connection segment and the right-angle steel and widened as the loading progressed. The connection segment bent obviously, and its paint coating peeled off in a large area at that time. The end of the connection segment fractured at the loading displacement with a length of −12 mm ($\delta^{-}=1/147$). The width–thickness ratio of stiffener increased, resulting in the asymmetry of the bending deflection of the connection segment, which may explain the difference between the CBRB-1 and the CBRB-2.

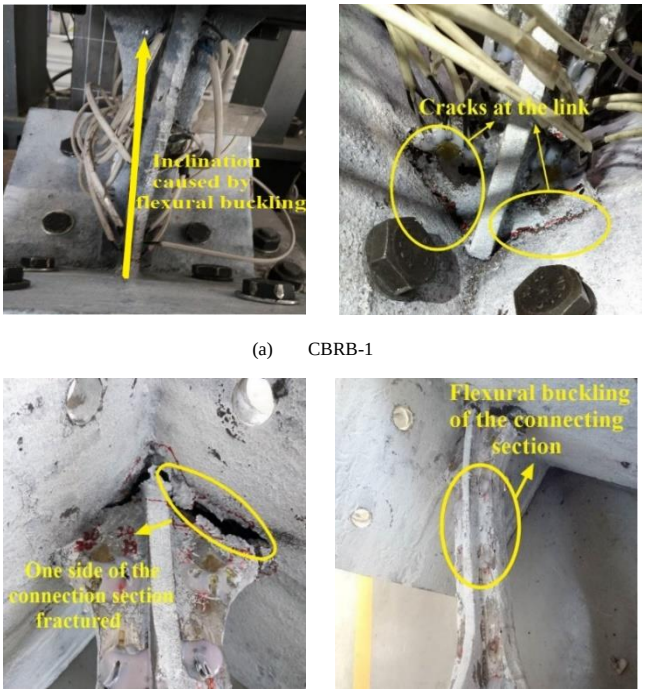

Fig. 9 Failure modes of Group 1 specimens at the final stage

The second set of tests examined the performance of the improved specimens, and all showed similar phenomena. The tension and compression deformation of all specimens had a fairly stable growth with the increase in loading displacement. No significant bending of connection segment was found during the test loading process, which is consistent with the smaller out-of-plane displacement than that of the Group 1 specimens, as detected by the Nos. 9 and 10 transverse displacement meters. These findings suggest that an improved method of increasing the width–thickness ratio of energy dissipation plate and stiffener may help prevent the local buckling of connection segments effectively. The selected typical test phenomena of CBRB-4 are further discussion in detail. At a loading displacement of 12 mm ($\delta^{\pm}=1/147$), the exposed part of the inner tube at the lower end of the BRB showed a slight swelling of paint (Fig. 10a). The same phenomenon with a few cracks of paint was found near the weld of BRB and flange plate at the upper end (Fig. 10b). The order of specimens observed these findings is as follows: CBRB-8, CBRB-7, CBRB-3, CBRB-4, CBRB-5, and CBRB-6. This finding suggests that a smaller axial force overstrength coefficient means that the BRB enters the plastic stage at a later point. These findings were not obvious in the first set of testing. Overall, these results demonstrate that the improved cast connector can better maintain the plastic deformation and damage accumulation of BRB. As shown in Fig. 10c, the coating paint of the energy dissipation segment of the CBRB-4 bulged slightly as the compression rate reached approximately 1/126. Some were accompanied by slight coating cracks, such as CBRB-7 and CBRB-8. As the test continued, cracks in the paint skin at the energy dissipation segment of each specimen began to develop and increase in number gradually. Also, the upper exposed part of the inner tube showed obvious bulging, and the lacquered skin of the lower exposed part began to peel off, as shown in Figs. 10d and 10e, respectively. Only a few cracks appeared at the connection segment, and no crack appeared at the link between the angle steel and the end of the connection segment unlike with the Group 1 specimens even though it was also detected some out-of-plane displacements of the members. The results indicate that end reinforcement may help prevent fracture due to the buckling of the connection segment. When the displacement was about 18 mm ($\delta^{+}=1/98$), the bearing capacity of CBRB-3 was reduced, the inner tube bulged seriously, and the loading stopped. When the elongation rate was about 1/88, the bearing capacity of CBRB-4 and CBRB-6 was reduced. The bearing capacity of CBRB-8 decreased at the displacement of −24 mm ($\delta^{-}=1/73$), while that of CBRB-5 and CBRB-7 decreased until the displacement reached 26 mm ($\delta^{+}=1/68$). The striking aspect of the results is that the improved specimen has better ductility and stronger deformability.

The failure mode of the Group 1 specimens belongs to the fracture caused by cracks of the cast connector end due to the flexural buckling of the connection segment. A possible reason may be that the smaller width–thickness ratio of the stiffener and energy dissipation plate led to the flexural buckling of

the connection segment under compressive loading. Another reason for this condition is that a weak link may exist between the energy dissipation plate and the angle steel because the end was not poured tightly. As can be seen from Fig. 9d, cracks produced easily in the weak link, resulting in fracture under eccentric loading caused by the out-of-plane inclination of the specimen, especially after bending of the connection segment. Unlike the Group 1 specimens, the Group 2 specimens did not exhibit a significant bending deflection of the connection segment (Fig. 10f). A large number of paint cracks were found at the energy dissipation segment. Moreover, the bulge at the exposed part of the inner tube indicated that local buckling had occurred. These results provide further support for the idea that the ductility of all members of improved specimens was fully utilized. The tests ended with the decreased bearing capacity of these specimens, and the low cycle fatigue is their main failure mode.

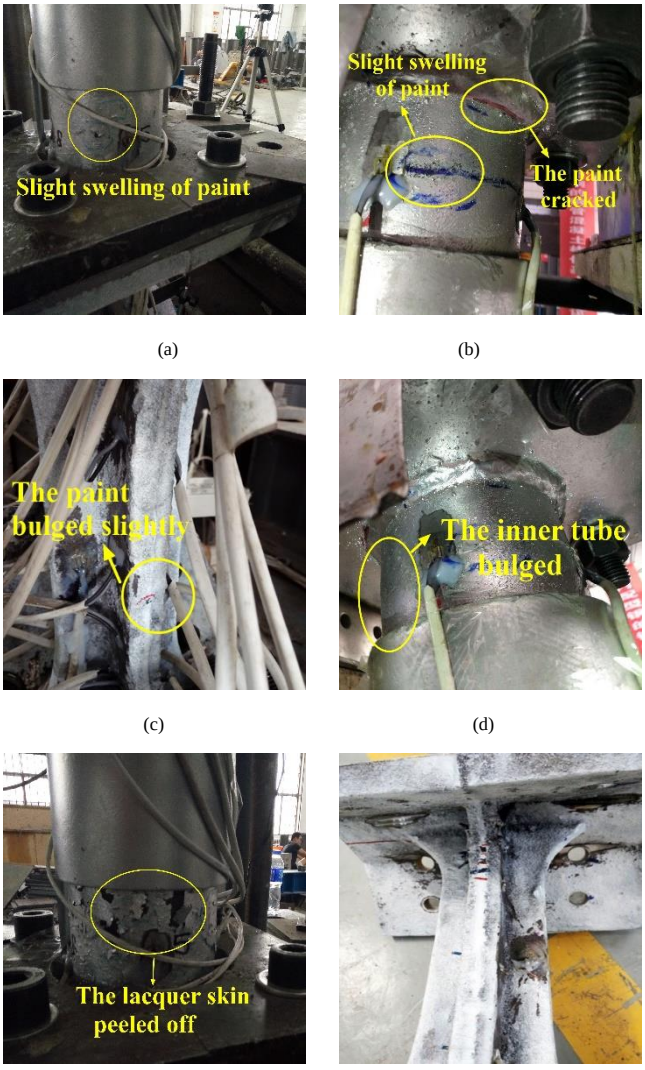

Fig. 10 Failure modes of CBRB-4 in Group 2

4.2. Deformation analysis

Fig. 11 provides the axial deformation of all specimens under the peak displacement of tension and compression load from the reading of vertical displacement meters. The entire deformation of the specimen is controlled by the ductile cast connector and the inner tube of BRB. The percentage of cast connector deformation in total deformation of the Group 1 specimens varies from 50% to 83%, while that of the Group 2 specimens varies from 59% to 92%. This finding suggests that most of the deformation of the specimen is mainly concentrated on the cast connector. The most obvious finding is that the energy dissipation time of the Group 2 specimens is longer, and the loading displacement of the cast connector deformation is significantly larger than that of the Group 1 specimens, which indicates that the cast connectors of the improved specimens have better plastic deformation and accumulation ability. Another important finding is that the displacement exerted by the actuator from the start of loading in the test of Group 1 specimens is significantly larger than the axial entire deformation of the specimen and is more obvious under compressive load. This inconsistency may be due to different degrees of flexural buckling of cast connectors, which caused the specimen to tilt and produce non-axial displacement. This result agrees well with the test phenomena of the first set. The occurrence of this phenomenon in the second set is obviously delayed, and the maximum non-axial displacement is 61% lower than that in the first set. The data from this figure can be combined with the data in Fig. 12, which shows the out-of-plane displacements of cast connectors along the x-axis (energy dissipation plate) and y-axis (stiffener) under compressive load from the readings of the Nos. 9 and 10 displacement meters. Notably, the local buckling of the Group 2 specimens occurs after 8 mm loading displacement ($\delta^{+}=1/220$), and the bending degree in two directions is reduced compared with that of the Group 1 specimens. These results further indicate that the improved method of increasing the width–thickness ratio of stiffeners and energy dissipation plates can slow down the flexural buckling degree of cast connectors. Interestingly, no difference is found in the width–thickness ratios of the energy dissipation plate between the CBRB-1 and CBRB-2, whereas the x-axis deformation of CBRB-1 decreases by 41% on average compared with CBRB-2. This finding is unexpected and suggests that a larger width–thickness ratio in a certain axial direction corresponds to larger deformation in the axis of symmetry.

In the range of tensile and compressive rates from 1/880 to 1/440, the percentage of the deformation of the cast connector to the total deformation of the specimen increases with the loading displacement, and the inner tube of BRB is in the elastic deformation stage. After the loading displacement of 4 mm, Fig. 11 shows that the percentage of the axial deformation of the cast connector to the total deformation exhibits a clear trend of decreasing first and then increasing gradually. This result can be explained by the rapid increase in the deformation of the BRB inner tube caused by the overstrength effect of the parts of the energy dissipation segment that has entered the plastic phase. The ratio of the cross-sectional area of the energy dissipation segment to the inner tube of the BRB in this test was controlled within the range of 0.595 to 0.957. Therefore, the cast connector and the BRB are connected in series, ensuring that the energy dissipation segment can yield before the inner tube during the axial force transfer in this bracing system. The hardening of the energy dissipation segment is similar to turning on the energy dissipation switch of the BRB, causing the inner tube to perform supplementary energy dissipation, thus achieving a two-stage energy dissipation mechanism. Subsequently, the deformation of the inner tube gradually stabilized after yielding, while the deformation of the cast connectors continued to grow steadily. These results show that the cast connector can ensure the BRB dissipates energy continuously and stably. At the late loading stage of Group 1 specimens, the percentage of cast connector deformation of CBRB-1 and CBRB-2 in total deformation are maintained at about 69% and 59%, respectively. The percentage of the deformation of cast connectors in the total deformation of Group 2 specimens is still increasing steadily, and evidence that the deformation of cast connectors can reach 82% of the entirety of component deformation on average is found when the specimens were damaged. Overall, these results further support that the improved cast connector has better ductility and stable energy dissipation.

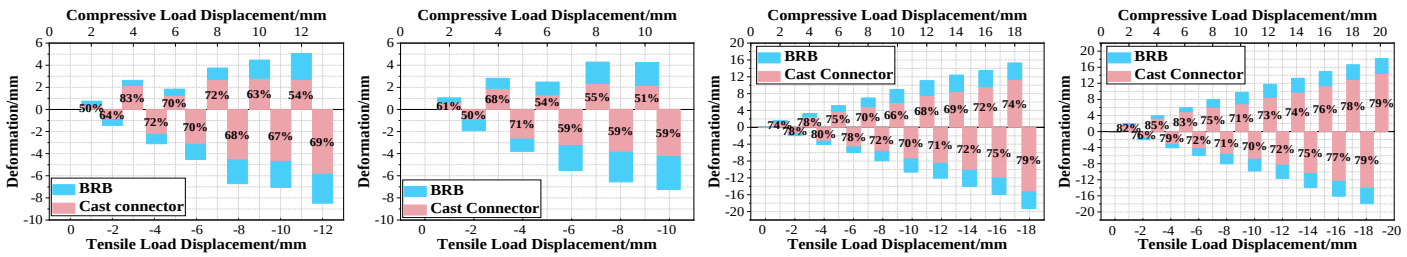

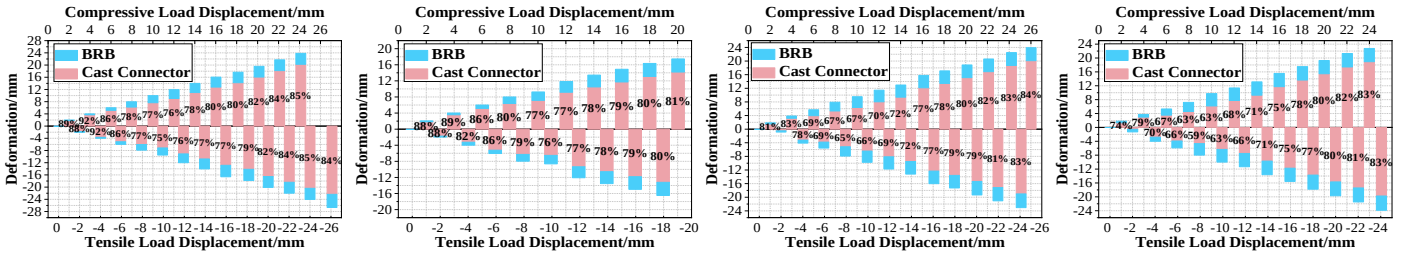

(e) CBRB-5 (f) CBRB-6 (g) CBRB-7 (h) CBRB-8

Fig. 11 Axial deformation of specimens

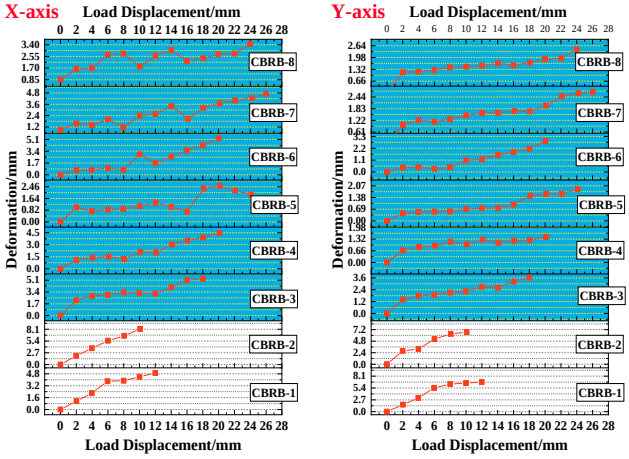

(a) (b)

Fig. 12 Deformation trend diagram of energy dissipation plates and stiffeners

We now focus on experimental evidence of the influence of design parameters on the deformability of members. A striking observation from the data comparison is that the axial deformation of cast connectors from CBRB-3, CBRB-4, and CBRB-5 increased in turn under the pressure at each loading stage, which is likely to be related to the length of the energy dissipation segment. Interestingly, the differences between displacement exerted by the actuator and the entire deformation of the specimen are highlighted with the decrease in the length of the energy dissipation segment. The higher non-axial displacement may be due to the decrease in the stiffness of the cast connector with the length of the energy dissipation segment, and a larger stiffness easily causes instability of the end for the cast connector. This finding indicates that the long energy dissipation segment can delay the local buckling of the connection segment. A closer inspection of Fig. 11 shows that the inner tube of BRB deforms more and tends to stabilize relatively later with the overstrength coefficient of the axial force. This finding matches the order of specimens where paint swelling was observed among the test phenomena. The reason for this special phenomenon is that the large overstrength effect of the cast connector causing the assembled BRB to enter the plastic stage early. The correlation between the deformation of the cast connector and the overstrength coefficient is interesting because the deformation of the cast connector decreases at the early stage and increases at the middle and late stages of loading with the overstrength coefficient. A clear benefit of increasing the overstrength coefficient in the development of plastic deformation of the energy dissipation segment can be identified in this analysis.

4.3. Stress distribution

The stress on each component of the specimen is calculated according to Hooke's law by using the strain from results measured by the strain collection device, and the yield mechanism for components can be determined by whether the stress value is currently above or below the yield strength. No significant difference was found among the stress distribution rules of eight specimens. Therefore, only the member stresses of CBRB-1 and CBRB-6 under different loading displacements are considered, as shown in Fig. 13, to facilitate the illustration of some main characteristics of the stress distribution for two sets of specimens. The stress of each part of the specimen is very small at δ=1/880, and the global specimen is in the elastic stage at this time. Afterward, the specimen is in the elastoplastic stage at δ^{+}=1/293. Notably, the stress value of L2 exceeds the yield strength, that is, the energy dissipation segment occurs the inelastic deformation to dissipate energy at the moment, while the rest of the components are maintained in the elastic phase. The stress of the connection segment (L1) of CBRB-6 is far less than the yield stress and is compared with that of CBRB-1, which reached the yield strength under compressive load. This disparity implies that the improved specimen can better alleviate stress concentration of the joint connected with the right-angle support. In addition, the stress difference between the energy dissipation segment and the BRB inner tube at δ=1/293 loading displacement is significantly increased compared with that at δ=1/880. This condition was sufficient to demonstrate that the inner tube starts to participate in energy dissipation at this time. Furthermore, the tensile and compressive stresses of each part of the specimen are inconsistent especially in the L1 from δ=1/293 onwards. The stress under pressure load is significantly greater than that under tension load, which indicates that material hardening occurs under the pressure load. The energy dissipation segment entered the full section, dissipating energy as the δ reached 1/176, whereas the stress of the connection segment and the transition segment of CBRB-6 were both still in the elastic stage. A detail that should be clarified is that the stress of the inner tube increases obviously as the stress difference between the energy dissipation segment and BRB begin to decrease. An implication of this condition is that the cast connector and the BRB are jointly involved in energy dissipation at this time. The stress in the energy dissipation segment increases continuously due to the effect of the overstrength. Fig. 13b clearly shows that the stress of the inner tube of CBRB-6 exceeded the yield load to dissipate energy at δ=1/147, where both L1 and L3 remained in the elastic phase and the stress variation began to level off. As a corollary, even when the energy dissipation segment of the cast connector increased closer to the ultimate strength, corresponding to the transition segment, it can stably transfer load and the connection segment can alleviate the stress concentration of the connection that is connected with the frame. The fracture of the specimen CBRB-1 occurred due to flexural buckling of the connection segment at δ^{-}=1/147, which matches the observation that the stress value of the L1 is close to that of L2, but BRB had not yet yielded.

Significantly, the energy dissipation segment (L2) is the region of maximum stress for the whole specimen in any loading phase, which suggests the feasibility of protecting the other components by weakening the cross-section of L2 to concentrate most of the stresses in the energy dissipation segment. The stress distribution result shows that the L1 and L2 of the improved cast connector are consistently maintained in elasticity, which ensures stable force transmission in the CBRB system while avoiding brittle fracture due to residual stress in traditional welded gusset plates. The energy dissipation segment of the cast connector first turns into plasticity and is followed by the inner core of BRB in a plastic state. This condition achieves the goal of the system to dissipate earthquake energy by stages.

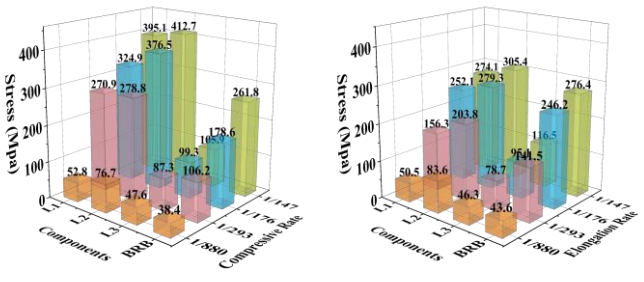

(a) CBRB-1

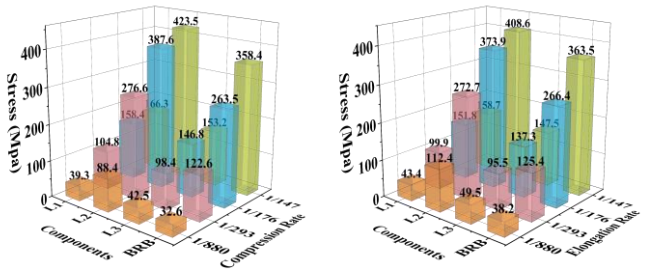

(b) CBRB-6

Fig. 13 Comparison of stress distribution of components for CBRB-1 and CBRB-6

4.4. Energy dissipation behavior

The key point of this research is to examine the energy dissipation capacity of specimen by utilizing hysteretic curves. Fig. 14 provides experimental loops for both loading histories of all specimens, where the hysteresis loop is very narrow during early cycles when the specimen is in the elastic stage and the energy dissipation is small. As the loading progresses, the specimen starts to dissipate large quantities of energy. Thus, the hysteresis loop becomes full. These curves shows a slight slip spring as specimens under tensile–compressive transformation are noticeable. A possible explanation for this condition may be that certain gaps are inevitably left during the assembly of each component. The hysteresis loop of the improved specimen is full, in which the ultimate bearing capacity increases loop by loop and the energy dissipation performance is better than that of the hysteresis loops of the specimens CBRB-1 and CBRB-2, which exhibit a scattered distribution in curves. This discrepancy could be attributed to the flexural buckling that occurred before a large amount of energy was dissipated in the plastic stage for the Group 1 specimens, which leads to severe stiffness degradation of the cast connector. Tension–compression imbalance remains most marked in the early loading process.

Data of CBRB-3–CBRB-5 show that the hysteresis loop becomes long and narrow, exhibiting a more obvious pinching phenomenon as the length of the energy dissipation segment increases. The main cause for this condition is that the bending behavior gradually predominates axial behavior as the slenderness ratio of the energy dissipation segment increased. Another important finding is that the imbalances between the tension and compression loading worsened as the length of the energy dissipation segment increased. This condition happens in the long energy dissipation segment, which generates a certain buckling when compressed, resulting in a few softened regions that are not conducive to transfer tensile loads. The specific focus is that the total area of hysteresis loops increases with the length of the energy dissipation segment at that time for the same cross-sectional area of the energy dissipation segment. This idea suggests that the energy absorption capacity of the specimen benefited from the increasing length of the energy dissipation segment. To ensure that a certain axial deformation capacity of the cast connector can dissipate a large amount of energy without instability, the slenderness ratio of the energy dissipation segment should be maintained at 16.72–17.47. Remarkably, the hysteresis loop area increases with the increase in the axial force overstrength coefficient, but this result is not significant at CBRB-8 (n = 0.845). This special phenomenon occurred because the rigidity of the cast connector reached a level that caused the assembled BRB to become a weak member, thus resulting in local instability at the late loading stage, which is unfavorable to the continuous energy dissipation for the specimen. Therefore, the axial force overstrength coefficient should be set within a reasonable range to ensure the energy dissipation performance of cast connectors. The hysteresis loop area also tends to increase with the increase in the cross-section area of the energy dissipation segment. Also, with the influence of the axial force overstrength coefficient on the energy dissipation of the system in stages taken into consideration, the optimal ratio of the cross-sectional area of the energy dissipation segment to the cross-sectional area of the inner tube should be in the range of 0.924–0.954.

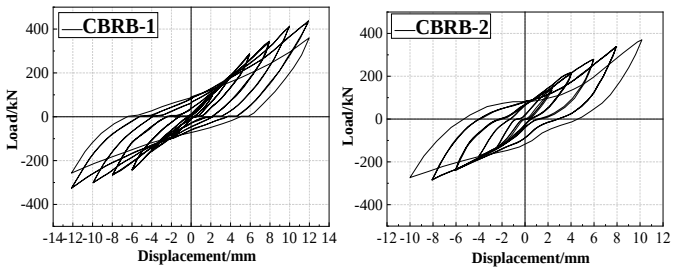

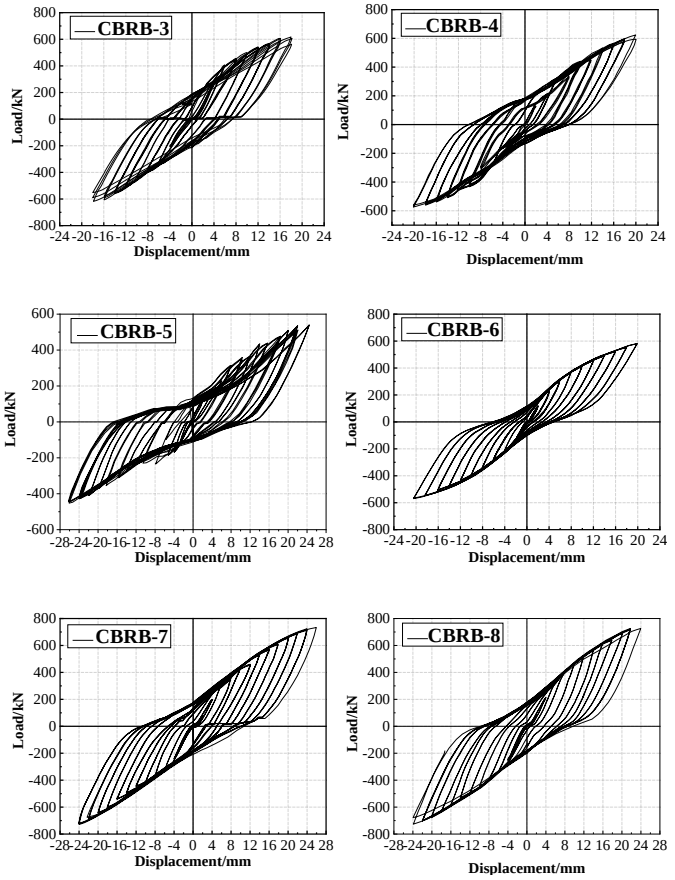

Fig. 14 Hysteretic curves of specimens

The energy dissipation coefficient, E , may have a large significance for the energy dissipation performance of the member, which can be obtained by the calculation diagram as shown in Fig. 15.

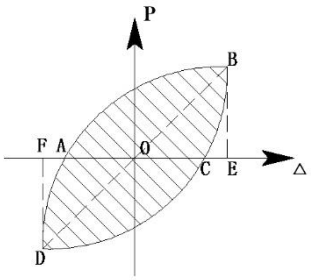

Fig. 15 Calculation diagram of energy dissipation coefficient E

where $S_{ABC+CDA}$ is the area enclosed by the hysteresis loops. $S_{\Delta OBE+\Delta ODF}$ is the sum of the areas of ΔOBE , and ΔODF can be calculated according to Equation (11)

$$E=\frac{S_{ABC+CDA}}{S_{\Delta OBE+\Delta ODF}} \tag{11}$$

Table 4 compares the energy dissipation coefficient of all specimens. The energy dissipation coefficient of the improved specimens is in the range of 1.23–1.48, which is larger than the energy dissipation coefficients of 1.06 and 1.18 of the specimens before the improvement. Evidence from this condition suggests that the improved method for reinforcing the end and improving the cross-shaped section area of the cast connector strengthens the energy dissipation performance of the specimens. Notably, data from CBRB-3–CBRB-5 show that the energy dissipation coefficient E increases with successive 50 mm increases in the length of the energy dissipation segment. Table 4 shows the positive correlation between the overstrength coefficient and energy dissipation capacity before the overstrength coefficient reaches 0.845. The overstrength coefficient affects the axial deformation of the cast connector observed in Fig. 11, yet its

increase will also increase the space for plastic development in the energy dissipation segment. These findings are in line with the data from the total area of hysteresis loops.

Table 4
The energy dissipation coefficient

Number	CBR B-1	CBR B-2	CBR B-3	CBR B-4	CBR B-5	CBR B-6	CBR B-7	CBR B-8
E	1.06	1.18	1.33	1.38	1.43	1.23	1.48	1.42

4.5. Skeleton curves

The ultimate bearing capacity of specimens identified in these cycle responses is presented in Fig. 16. The skeleton curves of the specimens with different parameters have a similar variation trend, including elastic, hardening, and plastic stages. The specimens are all elastically deformed within 4 mm displacement, and the ultimate bearing capacity basically increases linearly with displacement. The specimens entered the elastic–plastic stage, and the bearing capacity grows at a slower rate with loading displacements. In the plastic stage, the growth of the bearing capacity of the specimen was reduced obviously until the load finally reached the maximum. Notably, the displacement of Group 2 specimens entering the plastic stage is greater than that of the Group 1 specimens, thereby showing that the improved specimens have higher ductility. The results demonstrate that the process of increasing the width–thickness ratio of energy dissipation plate and stiffener and casting the right-angle tip tightly within a certain length of the cast connector is useful in developing the plasticity of the energy dissipation segment and increasing the bearing capacity of the member. For CBRB-3–CBRB-5, a clear trend of the decreased bearing capacity is found, along with the component entering the plastic stage later as the length of energy dissipation segments increases. Furthermore, the changing trend of bearing capacity for CBRB-3 and CBRB-4 is similar, where the curves come closest to coinciding in shape. Yet, the bearing capacity of CBRB-5, which has a long energy dissipation segment. is dramatically lower than that of CBRB-3 and CBRB-4, which have a short energy dissipation segment. These results represent the only a small part of the tension–compression region of the energy dissipation segment entering the plastic stage and reaches the ultimate strength where the bearing capacity is reduced significantly as the energy dissipation segment increases once a certain threshold of the slenderness ratio is achieved. The skeleton curves of the specimens CBRB-6, CBRB-4, CBRB-7, and CBRB-8 are symmetrical in compression and tension. The single most striking observation to emerge from the data comparison is that no significant differences were found in the development trend of skeleton curves of these specimens at the elastic stage and are followed by a positive correlation between the overstrength coefficient of axial force and bearing capacity at the plastic stage, as shown in Fig. 16c. This finding further confirms the association between the overstrength coefficient of axial force and bearing capacity, namely, that a high overstrength coefficient of axial force corresponds to a severe degree of plastic development of the energy dissipation segment.

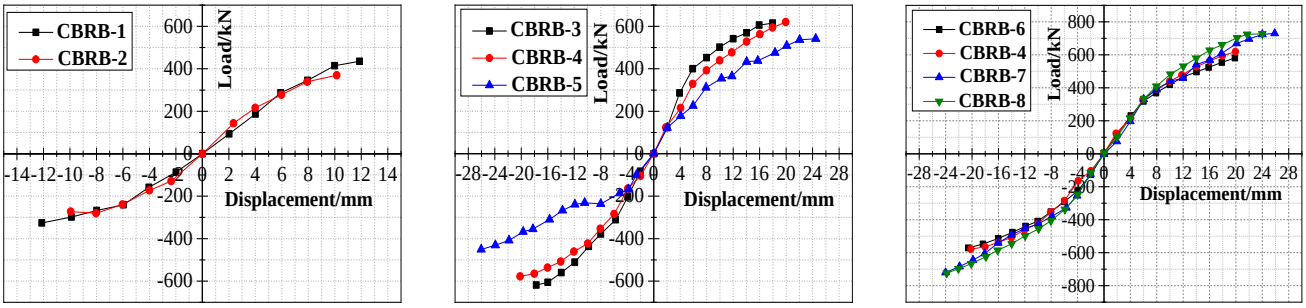

(a) CBRB-1 and CBRB-2 (b) CBRB-3~CBRB-5 (c) CBRB-6~CBRB-8

Fig. 16 Skeleton curves of specimens

4.6. Stiffness degradation

To further describe the degree of stiffness degradation of the specimen during the test, an average stiffness degradation curve is presented. The average stiffness is defined as the ratio of the sum of absolute values of tensile and compressive load peaks to the sum of corresponding displacement extremes. The average stiffness K_i can be expressed as

$$K_i = \frac{|P_i^+| + |P_i^-|}{|\Delta_i^+| + |\Delta_i^-|} \tag{12}$$

where $|\Delta_i^{\pm}|$ and $|P_i^{\pm}|$ are the extreme displacement and peak load in tension and compression at i loading cycle, respectively. Fig. 17 shows the summary of the stiffness degradation for each specimen. This figure clearly shows that the stiffness degradation rate at the initial stage of loading is fast, which corresponds to the fact that the cast connector bore the brunt of energy dissipation, and then gradually slows down as a result of the inner tube of BRB for supplementary energy dissipation. Afterward, the inner tube yielded and the cast connector entered the plastic stage, which corresponds to the slight acceleration of the stiffness degradation rate of the specimen. Fig. 17b also shows that the value of the initial stiffness of the specimen decreased with the increase in the length of the energy dissipation segment. No significant differences were found between stiffness degradation rates for these specimens at the initial stage of loading. The rigidity degeneration curve of CBRB-5 is less steep compared with that of CBRB-3 and CBRB-4 in the late loading stage, which may be due to the bending behavior gradually predominating the axial behavior of energy dissipation segment, thereby causing the slower development of plasticity. A closer comparison of the curves in Fig. 17c shows that the trend of stiffness degradation of those specimens is approximate, and the stiffness degradation trend appeared to be unaffected by the overstrength coefficient of axial force.

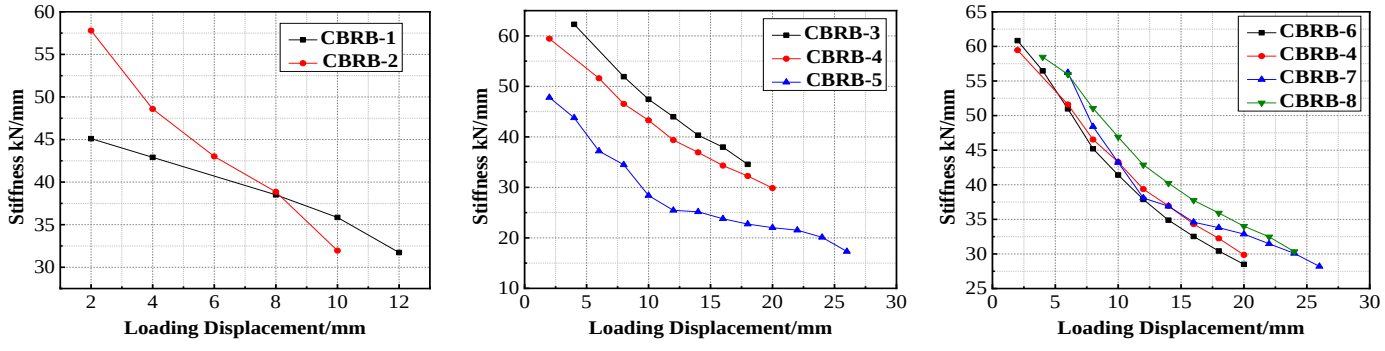

(a) CBRB-1 and CBRB-2 (b) CBRB-3~CBRB-5 (c) CBRB-4, CBRB-6~CBRB-8

Fig. 17 Stiffness degradation curves

5. Conclusions

A type of BRB with ductile cast connectors was developed to address the inability of the conventional brace system to fully perform energy dissipation due to premature buckling of the brace and the brittle fracture of the gusset plate. The seismic behavior of the proposed members was evaluated by testing two groups of full-scale specimens before and after improvement subject to cyclic loadings. The main parameters are the lengths of energy dissipation segment and axial force overstrength factors, and their influences on the seismic behavior of specimens were investigated. The major findings of this study are summarized as follows:

(1) The failure mode of the Group 2 specimens belongs to ductile failure, whereas the Group 1 specimens suffered brittle fracture at an early stage, thereby confirming that the improved method for reinforcing the end and improving the cross-shaped section area of the cast connector can help prevent the local buckling of connection segments and strengthen the seismic performance of the specimens effectively.

(2) The greatest axial deformation of the CBRB system was concentrated on the cast connector, which ensures continuous and steady energy dissipation for BRB. The maximum stress position of the whole specimen is in the energy dissipation segment, which maintains the connection and transition segments in an elastic phase at all times, thereby enabling the transition segment to transfer load stably and relieving the stress concentration in the connection segment, thus avoiding the fracture of the gusset plate of SCBFs.

(3) The increase in the length of the energy dissipation segment enhances the energy dissipation capacity of the specimen considerably, whereas the axial deformability and the bearing capacity are reduced with as the energy dissipation segment increases once a certain threshold of the slenderness ratio is achieved. The results of this study demonstrate that the members with energy dissipation segments with slenderness ratios in the range of 16.72–17.47 have the best seismic performance.

(4) The axial force overstrength factor represents a space for plastic development in the energy dissipation segment, which is proportional to the cross-sectional area of the energy dissipation segment. However, an excessively large axial force overstrength factor is unfavorable for energy dissipation of the specimen in stages and should be less than 0.845. The optimal ratio of the cross-sectional area of the energy dissipation segment to that of the inner tube should be in the range of 0.924–0.954.

(5) All specimens showed obvious stiffness degradation, and the stiffness degradation law is closely related to the phased energy dissipation of the member. A longer energy dissipation segment corresponds to a lower value of the initial stiffness of the specimen.

This study provides a comprehensive assessment of the seismic performance of buckling-restrained brace with ductile cast connectors, and the findings of this research provide insights for future work into assembly ductile connectors of bracing systems. A limitation of this study is that the cast connector is made of Q235 steel, and more research using controlled tests is needed for cast connectors made of different materials, such as low-yield-point steel. Unfortunately, although the increase in the length of the energy dissipation segment improves the energy absorption capacity to a certain extent, it also enhances the bending behavior. To address this issue, an effective way is to use a ferrule to add to the energy dissipation segment of the ductile cast connector to improve the axial compression behavior of the long energy dissipation segment. Further studies are needed to validate whether this measure can improve the stability of the energy dissipation segment to reduce the effect of the excessively long energy dissipation segment on the energy dissipation of the CBRB system.

Acknowledgment

Financial support for this research is provided by the National Natural Science Foundation of China (51968044, 51568040) and the National Key R&D Program of China (2019YFD1101003). Test conditions were supplied by the Engineering Research Center of the Ministry of Education for Earthquake Prevention and Disaster Reduction of Civil Engineering in Western China.

References

[1] Sabelli R., Roeder C.W. and Hajjar J.F., “Seismic design of steel special concentrically braced frame systems: a guide for practicing engineers”, NEHRP Seismic Design Technical Brief No.8, Gaithersburg, MD, 2013.
[2] Park R., Billings I.J., Clifton G.C., Cousins J. and Walker G., “The Hyogo-Ken Nanbu earthquake (the Great Hanshin Earthquake) of 17 January 1995”, Bulletin of the New Zealand Society for Earthquake Engineering, 28(1), 1-98, 1995.
[3] Astaneh-Asl A., Goel S.C. and Hanson R.D., “Cyclic out-of-plane buckling of double-angle bracing”, Journal of Structural Engineering, 111(5), 1135-1153, 1985.
[4] Goel S.C. and El-Tayem A.A., “Cyclic load behavior of angle x-bracing”, Journal of Structural Engineering, 112(11), 2528-2539, 1986.
[5] Rabinovitch J.S. and Cheng J.J.R. “Cyclic behavior of steel gusset plate connectors”, Structural Engineering Report No. 191, University of Alberta, Alberta, Canada, 1993.
[6] Cheng J.J.R, Yam M.C.H. and Hu S.Z., “Elastic buckling strength of gusset plate connectors”, Journal of Structural Engineering, 120(2), 538-559, 1994.
[7] Brown V.L.S. Stability of gusseted connections in steel structures, D.E., Department of Civil Engineering, University of Delaware, Delaware, USA, 1998.
[8] Walbridge S.S., Grondin G.Y. and Cheng J., “An analysis of the cyclic behaviour of steel gusset plate connections”, Journal of Constructional Steel Research, 46(1), 449-450, 1998.
[9] Sheng N., Yam C.H. and Lu V.P., “Analytical investigation and the design of the compressive strength of steel gusset plate connections”, Journal of Constructional Steel Research, 58(11), 1473-1493, 2002.
[10] Tremblay R., “Inelastic seismic response of steel bracing members”, Journal of Constructional Steel Research, 58(5), 665-701, 2002.
[11] Shaback B. and Brown T., “Behaviour of square hollow structural steel braces with end connections under reversed cyclic axial loading”, Canadian Journal of Civil Engineering, 30(4), 745-753, 2003.
[12] Uriz P. and Mahin S.A., “Seismic performance assessment of concentrically braced steel frames”, Proceedings of the 13th World Conference on Earthquake Engineering, Vancouver, BC, Canada, 2004.
[13] Roeder C.W., Lehman D.E., Clark K., Powell J. and Wei C.Y., “Influence of gusset plate connections and braces on the seismic performance of X-braced frames”, Earthquake Engineering & Structural Dynamics, 40(4), 355-374, 2011.
[14] Roeder C.W., Lumpkin E.J. and Lehman D.E., “A balanced design procedure for special concentrically braced frame connections”, Journal of Constructional Steel Research, 67(11), 1760-1772, 2011.
[15] Lehman D.E. and Roeder C.W., “Improved Seismic Design of Concentrically Braced Frames and Gusset Plate Connections”, American Society of Civil Engineers Structures Congress, Vancouver, British Columbia, Canada, 1-10, 2008.
[16] Yoshino T. and Karino Y., “Experimental study on shear wall with braces: Part 2. Summaries of technical papers of annual meeting”, Architectural Institute of Japan, Structural Engineering Section, Tokyo, Japan, 11, 403-404, 1971.
[17] Clark P.W., Aiken I.D., Kasai K., Ko E. and Kimura I., “Design procedures for buildings incorporation hysteretic damping devices”, Proceedings of the 69th Annual SEAOC Convention, Sacramento, USA, 355–372, 1999.
[18] Nakamura H., Maeda Y. and Sasaki T., “Fatigue Properties of Practical-Scale Unbonded Braces”, Nippon Steel Technical Report, 82, 51-57, 2000.
[19] Koetaka Y., Narihara H. and Tsujita O., “Experimental study on buckling restrained braces”, Proceedings of the Sixth Pacific Structural Steel Conference, Beijing, China, 15-17, 2001.
[20] Wakabayashi M., Nakamura T., Kashibara A., Morizono T. and Yokoyama H, “Experimental study of elasto-plastic properties of precast concrete wall panels with built-insulating braces”, In: Summaries of Technical Papers of Annual Meeting, Architectural Institute of Japan, Structural Engineering Section, Tokyo, Japan, 10, 1041-1044, 1973.
[21] Mochizuki S., Murata Y., Andou N. and Takahashi S., “Experimental study on buckling of unbonded braces Under axial forces: Parts 1&2. Summaries of technical papers of annual meeting” , Architectural Institute of Japan, Structural Engineering Section, Tokyo, Japan, 1623-1626, 1979.
[22] Sridhara B.N., “Sleeved column-as a basic compression member”, Proceedings of the 4th International conference on steel structures and space frames, Singapore, 181-188, 1990.
[23] Iwata M., Kato T. and Wada A., “Buckling-restrained braces as hysteretic dampers”, Proceedings of the Behavior of Steel Structures in Seismic Areas: STESSA 2000, Montreal, Canada, 33-38, 2000.
[24] Xie L.Q., Wu J., Shi J.H. and Zhu Y.Q., “Influence of the core-restrainer clearance on the mechanical performance of sandwich buckling-restrained braces”, Advanced Steel Construction, 16(1), 37-46, 2020.
[25] Tada M., Kuwahara S. and Yoneyama T., “Horizontally loading test of the steel frame braced with double-tube members”, Annual Technical Papers of Steel Structures, 1, 203-208, 1993.
[26] Lai J.W. and Tsai K.C., “Research and application for buckling restrained braces in Taiwan”, 2004 ANCER Annual Meeting: The Sheraton Princess Kaiulani, Honolulu, Hawaii, 2004.
[27] Yin Z.Z. and Wang X.L., “Finite component analysis of constrained buckling support with contact ring”, Journal of Lanzhou University of Technology, 34(5), 122-126, 2008. (in Chinese)
[28] Yin Z.Z. and Bu F.C., “Overall stability analysis of improved buckling restrained braces”, The Open Civil Engineering Journal, 10(1), 61-75, 2016.
[29] Yin Z.Z., Chen W., Chen S.L. and Wang X.L., “Experimental study on buckling support of improved double steel tube”, Journal of Building Structures, 35(09), 90-97, 2014.
[30] Fleischman R.B., Sumer A. and Li X.J., “Development of modular connections for steel special moment frames”, American Society of Civil Engineers Structures Congress 2004, Nashville, Tennessee, United States, 1-9, 2004.
[31] Fleischman R.B. and Sumer A., “Optimum arm geometry for ductile modular connectors”, Journal of Structural Engineering, 132(5), 705-716, 2006.
[32] Oliveira J.C.D., Packer J.A. and Christopoulos C., “Cast steel connectors for circular hollow section braces under inelastic cyclic loading”, Journal of Structural Engineering, 134(3), 374-383, 2008.
[33] Gray M.G., “Cast steel yielding brace system for concentrically braced frames”, School of Graduate Studies - Theses, 2012.
[34] Khan K. and Yan J.B., “Numerical studies on the seismic behaviour of a prefabricated multi-storey modular steel building with new-type bolted joints”, Advanced Steel Construction, 17(1), 1-9, 2021.
[35] Hou Z.X., Gong C., Zhang Y., Sun Y.Z., Jiang J. and Li G.Q., “Seismic behavior of bolted connections with slot bolt holes at ambient and elevated temperature”, Advanced Steel Construction, 14(4), 651-667, 2018.
[36] Liu J.B. Theoretical study on design of anti-buckling support and buckling support frame, D.E., Tsinghua University, Beijing, China, 2005.
[37] GB50017-2003. Code for design of steel structures, China Architecture & Building Press, Beijing, China, 2006.
[38] GB/T 228–2002. Metallic materials-tensile testing at ambient temperature, China Standard Press, Beijing, China, 2002.